RSC Applied Interfaces

ROYAL SOCIETY OF CHEMISTRY

PAPER

View Article Online
View Journal | View Issue

Cite this: *RSC Appl. Interfaces*, 2024, **1**, 511

Ferrocene-labelled surfactants enhance the supercapacitor performance in PANI-PSS/nanocarbon layer-by-layer nanoarchitectonics electrodes†

Ana Paula Mártire, Gonzalo E. Fenoy, Omar Azzaroni, Matías Rafti and Waldemar A. Marmisollé *

Supercapacitors are devices that bridge the gap between traditional capacitors and rechargeable batteries, offering exceptional energy storage capabilities, rapid charge/discharge rates, long cycle life, and environmental friendliness. This study explores the development of neutral-aqueous supercapacitor materials using conductive polymers, with a focus on polyaniline (PANI) doped with anionic polyelectrolytes. Combining PANI with carbon nanomaterials through various construction processes, including layer-by-layer assembly, nanoarchitectonics is employed to create desirable nanostructures on the electrode surface. The introduction of a redox-active surfactant (ferrocene-labelled surfactant, FcCTAB) in the layer-by-layer assembly adds a unique dimension of redox activity, enhancing the electrochemical capacitance of the hybrid coatings. Through voltammetric, charge–discharge, and electrochemical quartz crystal microbalance (EQCM) measurements, we investigate the capacitive performance and dynamic mass changes during potential cycling. The study demonstrates that the integration of the redox moiety significantly improves capacitive performance in neutral solutions without compromising structural stability and cyclability. This approach synergistically combines nanocarbon materials, electroactive polymers, and the faradaic contribution of the electroactive surfactant, presenting a supercapacitor material with excellent performance with potential application in wearable devices for secure energy storage.

Received 29th November 2023,
Accepted 18th December 2023

DOI: 10.1039/d3lf00236e

rsc.li/RSCApplInter

Introduction

Among the various energy storage systems, supercapacitors have emerged as a promising and innovative technology that offers a compelling alternative to traditional batteries.[1] Supercapacitors possess unique characteristics that bridge the gap between conventional capacitors and rechargeable batteries.[2] These high-performance devices are gaining widespread attention due to their exceptional energy storage capabilities, rapid charge and discharge rates, long cycle life, and environmental friendliness.[3–5] Supercapacitors are devices consisting of two electrodes separated by an electrolyte solution. Two phenomena contribute to the capacitance of these devices: the electrochemical double layer and the redox chemical reactions. The first contribution comes from the charge distribution at each side of the interface.[2,6] The second one accounts for the occurrence of faradaic processes.[7]

Concerning the electrolyte solution, neutral aqueous solutions are environmentally friendly and readily available. By designing supercapacitor materials compatible with these solutions, we can promote sustainable energy storage technologies that minimize environmental impact.[8] This is especially crucial in the context of renewable energy systems, where the overall sustainability of energy storage technologies is highly desirable. On the other hand, compared to non-aqueous electrolytes, neutral aqueous solutions are generally less hazardous and more cost-effective. They have a lower risk of fire or explosion, making them safer for large-scale energy storage applications. Additionally, the cost and availability of water-based electrolytes are advantageous, enabling the development of affordable and scalable supercapacitor systems. Furthermore, neutral aqueous electrolytes facilitate the integration of energy storage devices for portable and wearable applications.

In this context, conductive polymers (CP) have a great combination of properties for constructing neutral-aqueous supercapacitor electrodes. In certain oxidation states conductive

Instituto de Investigaciones Fisicoquímicas Teóricas y Aplicadas (INIFTA), Departamento de Química, Facultad de Ciencias Exactas, Universidad Nacional de La Plata, La Plata B1904DPI, Argentina. E-mail: wmarmi@inifta.unlp.edu.ar, waldemarmarmisolle@quimica.unlp.edu.ar

† Electronic supplementary information (ESI) available: Additional material characterization, control experiments and complementary results. See DOI: https://doi.org/10.1039/d3lf00236e

polymers present a metal-like conductivity but with an upgraded surface area due to the polymer fibril network in contact with the electrolyte.[9,10] Particularly, polyaniline (PANI) has been often used in energy storage devices, due to its easy and low-cost synthesis and high stability and electroactivity in acidic solutions.[11] However, to prepare electrodes with enhanced neutral-aqueous-solution electroactivity, PANI is usually doped with anionic polyelectrolytes.[12] In this regard, PANI synthesized by template polymerization[13] in the presence of polystyrene sulfonate of sodium yields stable negatively charged dispersions of the complex PANI-PSS.[14]

Also, carbon nanomaterials are widely used in combination with diverse materials to upgrade the properties of the hybrid electrode in supercapacitor applications.[15–18] Particularly, the combination of carbon nanomaterials and PANI improves the electrochemical connectivity and the mechanical stability of the conductive polymer.[11,19] The rational design of an appropriate electrode–electrolyte interface applying these materials maximizes the capacitive performance making a profit from both carbon and PANI characteristics. Hence, nanoarchitectonics,[20,21] which is the concept of constructing desirable structures in the nanoscale, plays a key role in fabricating these electrodes.[22,23]

A diverse spectrum of construction processes combining carbon and PANI have been developed for supercapacitor applications.[19,24,25] On the one hand, the PANI-carbon composite is prepared prior to its deposition on the electrode surface. Within this approach, the integration of both materials can be performed by polymerization of PANI in the presence of the carbon material,[26] interfacial polymerization,[27] or directly mixing dispersions of both components.[28] On the other hand, the integration of PANI and carbon nanomaterials can be performed directly on the electrode surface. As an example, the electropolymerization of PANI from aniline solution is a method to controllably add the conducting polymer to a carbon-modified electrode.[29] Layer-by-Layer is another way to perform electrode modification by successively integrating positively and negatively charged building blocks.[30] Driven by intermolecular interactions, this controlled method generates an intimate contact between the building blocks and a regular hybrid 3D construction of the film.[31–33] In this regard, different kinds of carbons have been combined with PANI by the LbL approach for supercapacitor applications.[34–36]

The LbL technique requires a sufficiently stable dispersion of the building blocks. In the case of nanocarbons, this can be achieved by using dispersing agents, such as surfactants. In this regard, we have previously shown that stable dispersions of nanocarbons and 1-hexadecyltrimethylammonium bromide (CTAB) can be combined with PANI/PSS by an LbL approach to produce electroactive materials for energy storage applications.[35] In the present study, we explore the advantages of adding a redox moiety to this surfactant block. Thus, this study focuses on the development and electrochemical evaluation of LbL-assembled hybrid films comprising conductive polymer complexes (PANI-PSS) and surfactant-dispersed nanocarbon using an electroactive surfactant, a departure from the traditional role of surfactants that have primarily served as structural elements in the nanoarchitecture of the assembly.[37–40] The selected electroactive surfactant, ferrocene-labelled surfactant (FcCTAB), adds a unique dimension by introducing redox activity within the assembly[21] that would enhance the electrochemical capacitance of the hybrid coatings. Through a combination of voltammetric and charge–discharge experiments, we investigated the capacitive performance of assemblies with varying proportions of ferrocene-labelled surfactant. Moreover, the dynamics of the charge–discharge processes were studied by electrochemical QCM measurements. This study demonstrates that the integration of the redox moiety significantly enhances the capacitive performance of the hybrid material in neutral solutions without noticeably affecting its structural stability and cyclability.

Experimental section

Chemicals

Aniline, ammonium persulfate (APS), polyethylenimine (PEI) (50% in H_2O, Mw 750 kDa), poly (sodium 4-styrene sulfonate) (PSS) (Mw 70 kDa), and (1-hexadecyl)trimethyl-ammonium bromide 99%) (CTAB) were purchased from Sigma-Aldrich. Expanded graphite was purchased from Carbone Lorraine. (Ferrocenylmethyl)hexadecyldimethylammonium bromide (FcCTAB) was prepared in our laboratory following a protocol reported by Jeffrey Gold and coworkers.[41,42] Sulfuric acid, hydrochloric acid, and potassium chloride were purchased from Anedra. All chemicals were employed as received except for aniline, which was vacuum distilled. All solutions were prepared with deionized water (18.2 MΩ cm).

PANI-PSS synthesis

The PANI-PSS dispersion was prepared by chemical polymerization of a 5 mM aniline solution in 0.5 M HCl. Then, PSS was added to reach a concentration of 5 mM. After 15 minutes of stirring, APS was added to reach a 5 mM concentration, and the solution was stirred overnight. The synthesis was carried out in 40 mL falcon tubes, with a final synthesis volume of 20 mL. The preparation color was initially dark blue and then turned green. This dispersion was diluted 1/10 in 0.5 M HCl to be used in the LbL assembly.

Nanocarbon dispersion preparation

Nanocarbon dispersion was prepared by probe sonication of expanded graphite (1 mg mL^{-1}) in deionized water in the presence of surfactant at 0.5 mg mL^{-1} concentration as reported and characterized previously.[43] For the $x = 0$ and $x = 1$ systems, 0.5 mg mL^{-1} CTAB and FcCTAB were used, respectively. For the $x = 0.5$ dispersion, 0.25 mg mL^{-1} CTAB and 0.25 mg mL^{-1} FcCTAB were added. The solution was ultrasonicated for 30 minutes and subsequently diluted 1/50 in deionized water prior to use in the LbL assembly process (Fig. S1†).

Layer-by-Layer assembly

The LbL assembly was built on previously cleaned Au or glass substrates. In a typical process, the construction started with a 10-minute immersion of the substrates in a 1 mg mL^{-1} PEI solution followed by a 5 min-rinse in DI water. Then, the substrates were horizontally dipped in the PANI-PSS colloidal dispersion for 10 minutes. After the immersion in PANI-PSS, a 5 min-wash was performed with HCl 0.5 M. Then, the substrates were immersed in the nCs-CTAB (x = 0, 0.5, 1) dispersions and rinsed for 5 minutes in DI water. This sequence yielded a single bilayer, and n times repetitions were carried out to obtain a [PANI-PSS/nCs-CTAB (x = 0,0.5,1)]$_n$ multilayer assembly (Fig. 1A).

Characterization/electrochemical measurements

UV-vis spectroscopy. For the UV-vis measurements, the LbL assembly was prepared employing the bottom of beakers as substrates. Spectra were taken by using an Agilent model 8453E diode array spectrophotometer.

Electrochemical measurements. A Gamry Reference 600 potentiostat was used to measure the cyclic voltammetry and charge–discharge curves. A three-electrode setup was employed, using a Pt wire as the counter electrode and a Ag/AgCl (3 M NaCl) electrode as the reference. Au substrates, prepared by Au sputtering on glass, were used as working electrodes.

QCM measurements. Quartz crystal microbalance (QCM) measurements were performed with a QCM 200 (Stanford Research Systems) using gold-coated commercial quartz sensors (QCM25 5 MHz, sensitivity factor: 56.6 Hz cm^2 μg^{-1}). The LbL assembly procedure was performed on the sensors to measure the dry mass growth process. After that, the 11.5-bilayer assembly was analysed by eQCM experiments. To this end, the QCM 200 and the potentiostat were combined in the setup, employing a three-electrode arrangement in a Teflon cell while using a Pt wire and a Ag/AgCl (3 M NaCl) electrode as counter and reference electrodes, respectively.

Results and discussion

Layer-by-Layer assembly

The Layer-by-Layer technique was chosen to construct hybrid films integrating conductive polymer complexes (PANI-PSS) and surfactant-nanocarbon dispersions as depicted in Fig. 1A.

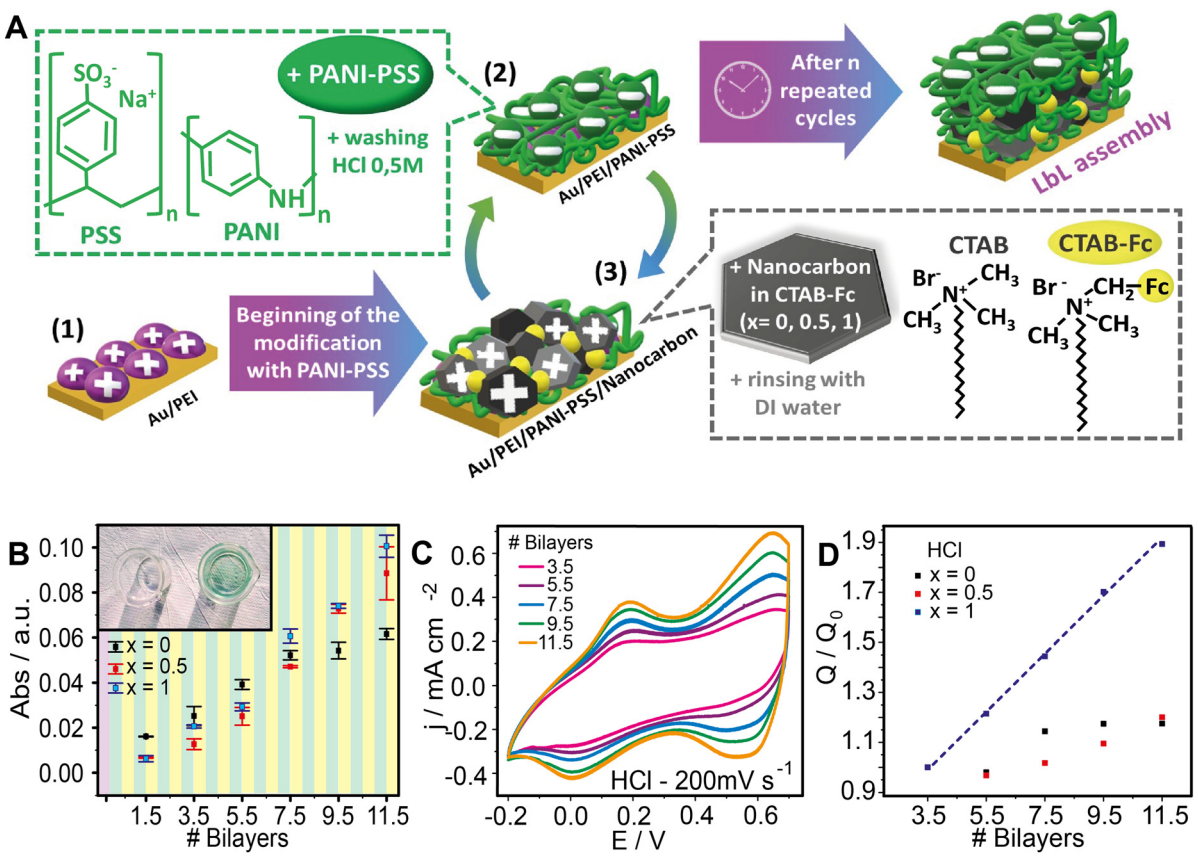

Fig. 1 (A) LbL assembly construction process scheme. (B) Absorbance at 750 nm monitored for three different assembly conditions as the number of bilayers increased. The bars correspond to the standard deviation of 3 different positions of the same beaker. Inset (B): picture of an unmodified (left) and a 11.5 bilayer-modified beaker (right). (C) Cyclic voltammograms of the assembly PANI-PSS/FcCTAB with different numbers of bilayers at 200 mV s^{-1} scan in an acidic medium (0.1 M HCl). (D) Relative charge calculated with 3.5 bilayer response as a reference. Cyclic voltammetry was performed in 0.1 M HCl at 200 mV s^{-1} scan rate.

Nanocarbon was dispersed using CTAB with or without ferrocene as a surfactant. To evaluate the ferrocene contribution to the response, three systems with different proportions of ferrocene-labelled surfactant were prepared and their growth and electrochemical responses were compared. For the first system, the nanocarbon was dispersed using only CTAB (without ferrocene moieties, $x = 0$); in the second assembly, an equal mixture of CTAB and FcCTAB was used ($x = 0.5$). In the third assembly, the nanocarbon was dispersed using only FcCTAB ($x = 1$) (Fig. S1†).

Next, the film growth was studied by UV-visible spectroscopy. To this end, the LbL films were prepared on the bottom of 5 mL beakers to ensure the horizontality of the LbL construction. As the PANI-PSS complex exhibits maximum absorption at 750 nm, the absorbance at this wavelength was monitored. It is observed that the absorbance increases after each deposition cycle, indicating a nearly linear increase in the amount of material added to the assemblies (Fig. 1B).

The LbL assemblies were also characterized by Raman, FTIR and SEM (see the ESI†). Raman spectra confirmed the presence of the conducting polymer block in the coatings for the three different assembly compositions (Fig. S2†). The FTIR spectra evidenced the presence of the surfactant block in the composed films (Fig. S3†). To have further information about the distribution of the film components in the Au surface, SEM images were taken from the 11.5 bilayer assemblies (Fig. S4†). A complete coverage of the surface with PANI-PSS was observed with nanocarbons inserted in the polymer matrix.

Electrochemical behavior of the LbL assemblies

Film electroactivity and electrochemical interconnection. The electroactivity and electrochemical interconnection of the LbL films were tested by performing cyclic voltammetry measurements after different stages of the construction procedure. To this end, the assembly was performed *in situ* in the electrochemical cell and cyclic voltammograms were recorded after the deposition of 3.5, 5.5, 7.5, 9.5, and 11.5 bilayers. Fig. 1C shows cyclic voltammograms for an increasing number of bilayers using only the ferrocene-labelled surfactant ($x = 1$). It can be seen that the current increases with the number of deposition cycles, implying the deposition of the electrochemically connected material.

Next, to evaluate the ferrocene-labelled surfactant contribution to film connectivity, this system was compared with one prepared using CTAB ($x = 0$) and 1 : 1 CTAB : FcCTAB ($x = 0.5$) as dispersing agents for the nanocarbon. The relative integrated charge was calculated for each system, taking 3.5 bilayer response as a reference (Fig. 1D). The integrated charge linearly increases with the number of deposition cycles for the PANI-PSS/FcCTAB construction ($x = 1$), proving good electrochemical connectivity within the assemblies. An increment of the integrated charge was also observed in assemblies $x = 0$ and $x = 0.5$, although the relative values were much lower than those observed for the assembly with $x = 1$.

On the other hand, the effect of the presence of the carbon nanomaterial within the assemblies on the electrochemical response was assessed.[44,45] In this regard, the assemblies without nanocarbon in the CTAB dispersion produced low voltammetric currents without a noticeable increment with the number of deposition cycles (Fig. S5†), accounting for the importance of the nanocarbon block on the electrochemical connection of the assemblies.

To evaluate the ferrocene contribution to the electrochemical performance of the three assemblies with different ferrocene-labelled surfactant proportions ($x = 0$, 0.5, and 1), electrodes with 11.5-bilayer assembly were constructed (Fig. 2A). The cyclic voltammetry response of these assemblies was analyzed with no measurement interruption during the growth procedure. Fig. 2B and C show the cyclic voltammetry response of the three systems in acidic and neutral solutions. It can be observed that the voltammetric current increases with the proportion of the ferrocene-labelled surfactant used in the assembly process. The contribution of the ferrocene/ferricenium moiety redox couple can be identified at about 0.5 V, as previously reported,[46] and it clearly increases the voltammetric integrated charge of the film-coated electrodes.

Aiming to quantify the change in the voltammetric response, the specific capacitance ($C_{CV,SP}$/F g^{-1}) was calculated according to the following equation (eqn (1)):

$$C_{CV,SP} = \frac{1}{m\nu(V_f - V_i)} \int_{V_i}^{V_f} I(V)\mathrm{d}V \quad (1)$$

where ν is the scan rate (V s^{-1}), V_i and V_f are the initial and final scanning potentials (V), I is the current measured (A) and m (g) is the deposited mass of the electroactive composite.

Next, in order to determine the deposited dry mass of the coatings, QCM measurements were performed. The evolution of the dry mass was assessed by depositing the LbL assembly on QCM sensors with the same protocol used for the Au electrodes (Fig. 2D). As observed for the UV-vis measurements, the results show that the amount of deposited material increases as the number of deposition cycles increases for all the assemblies with different proportions of ferrocene-labelled surfactants.

Using dry mass values for the 11.5-bilayer assemblies, the specific capacitances were calculated from the voltammetric responses in Fig. 2B and C. From Fig. 2E it can be observed that the specific capacitance of the composite-coated electrodes increases with the proportion of ferrocene-labelled surfactants. This can be ascribed to the incorporation of the redox moiety into the LbL assemblies, whose redox switching increases the overall composite capacitance.[7]

Moreover, measurements in acidic solution showed an improved response compared with those performed in neutral solutions, as expected from the enhanced electroactivity and conductivity of the PANI building block in acidic media.[47] Nevertheless, the assemblies still presented a good retention of the electroactivity (and therefore, the capacitance) in a neutral medium. The assemblies fabricated with $x = 1$ showed the highest capacitance: 138.4 F g^{-1} and 95.6 F g^{-1} in HCl and KCl

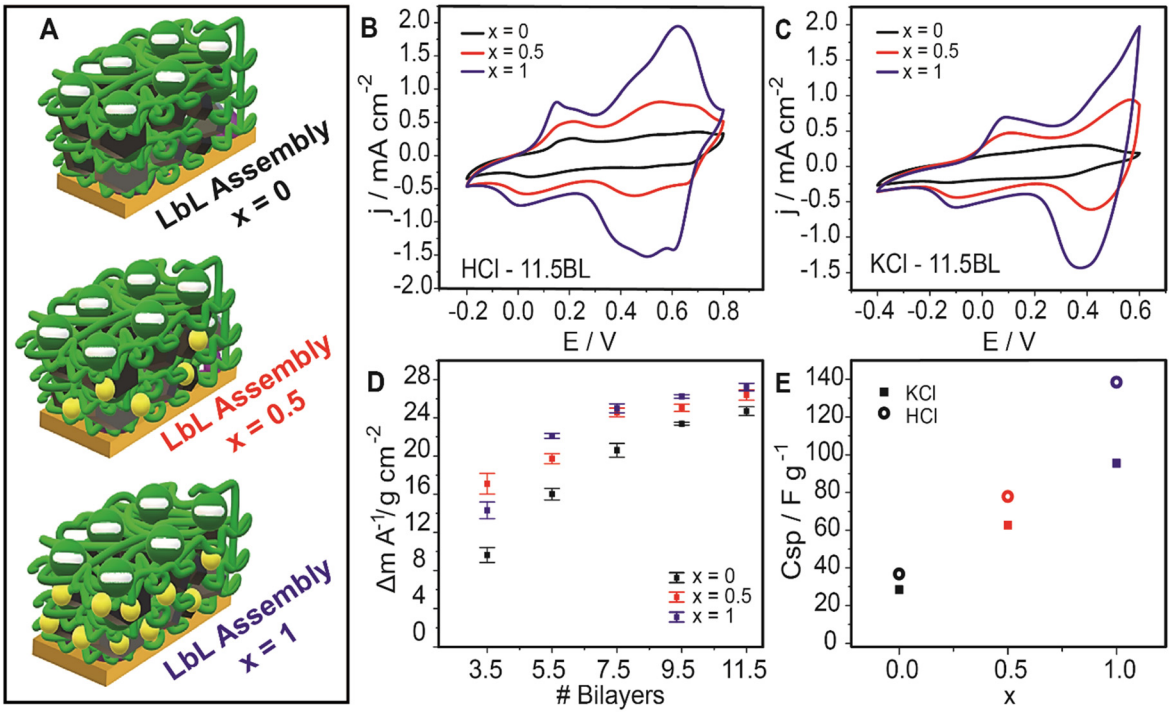

Fig. 2 (A) Scheme of the assemblies constructed for the three systems. Cyclic voltammograms of the three assemblies with different proportion of the ferrocene-labelled surfactant (x = 0, 0.5, and 1) at 200 mV s^{-1} (B) in acidic medium (0.1 M HCl) and (C) neutral medium (0.1 M KCl). (D) QCM dry mass measurements at different stages of the LbL assembly process. (E) Specific capacitance values at 200 mV s^{-1} for the 11.5-bilayer assembly in 0.1 M HCl and 0.1 M KCl.

0.1 M respectively (at 200 mV s^{-1}). For x = 0.5, the obtained $C_{CV,SP}$ values were 77.9 F g^{-1} and 62.8 F g^{-1} in 0.1 M HCl and KCl, respectively, whereas it was correspondingly 36.8 F g^{-1} and 26.5 F g^{-1} for x = 0. According to these values, the specific capacitance is increased by 124% from x = 0 to x = 0.5 and 268% from x = 0 to x = 1 averaging KCl and HCl performances. These results demonstrate that the incorporation of redox moieties into the nanocarbon-surfactant building block greatly enhances the electrochemical performance of the assemblies in terms of charge accumulation.

To study the reproducibility of the assembly fabrication protocol and their electrochemical performance, two additional sets of assemblies were built from new nanocarbon dispersions and PANI-PSS synthesis batches. Results confirm that the incorporation of ferrocene moieties in the surfactant structure leads to an increase in the capacitive response, both in acidic and neutral media (Fig. S6†). There is, however, some dispersion of $C_{CV,SP}$ values probably due to some differences in the exfoliation of the nanocarbon with the surfactant and the assembly of the different building blocks from different batches.

Electrochemical switching of the composite material. In order to study the electrochemical performance of the deposited assemblies in more depth, cyclic voltammograms were recorded for 11.5 bilayer-modified electrodes for the three systems at different scan rates from 10 to 1000 mV s^{-1} in both acidic and neutral media. Fig. 3A and B show the obtained CV curves and the peak current analysis for both 0.1 M HCl and 0.1 M KCl, respectively (note the differences in the current density scale for each system).

A typical response for PANI-PSS redox couples is observed in Fig. 3A and B for x = 0. In 0.1 M HCl, the first peak around 0.1 V corresponds to the leucoemeraldine/emeraldine transition and the last peak around 0.65 V corresponds to emeraldine/pernigraniline redox transition.[48,49] The peak in between these two could be assigned to the degradation products of PANI during the electrochemical cycling.[50] In 0.1 M KCl, peaks are less defined because they move closer to more negative potentials as the pH of the electrolyte increases.[51]

The ferrocene-labelled-surfactant response during cyclic voltammetry can be identified in Fig. 3A and B for x = 0.5 and 1. The reversible electron transfer between the ferrocene redox couple (Fe^{2+}/Fe^{3+}) is assigned to an outstanding peak approximately at 0.5 V which overlaps with the PANI electroactive response.[42] It can be also remarked that this peak increases from x = 0.5 to x = 1 with increasing ferrocene-labelled surfactant amount.

The peak current values were computed at about 0.2 and 0.5 V for HCl and 0.2 V for KCl. In all cases, a linear variation of the peak current as a function of the potential scan rate was observed, which is consistent with a surface-bounded electrochemical process without diffusion limitations[52] (insets in Fig. 3A and B).

For each voltammogram, the specific capacitance was calculated with eqn (1) for the different scan rates (Fig. 3C). The assembly with x = 1 showed the highest capacitance: 205.6 F g^{-1}

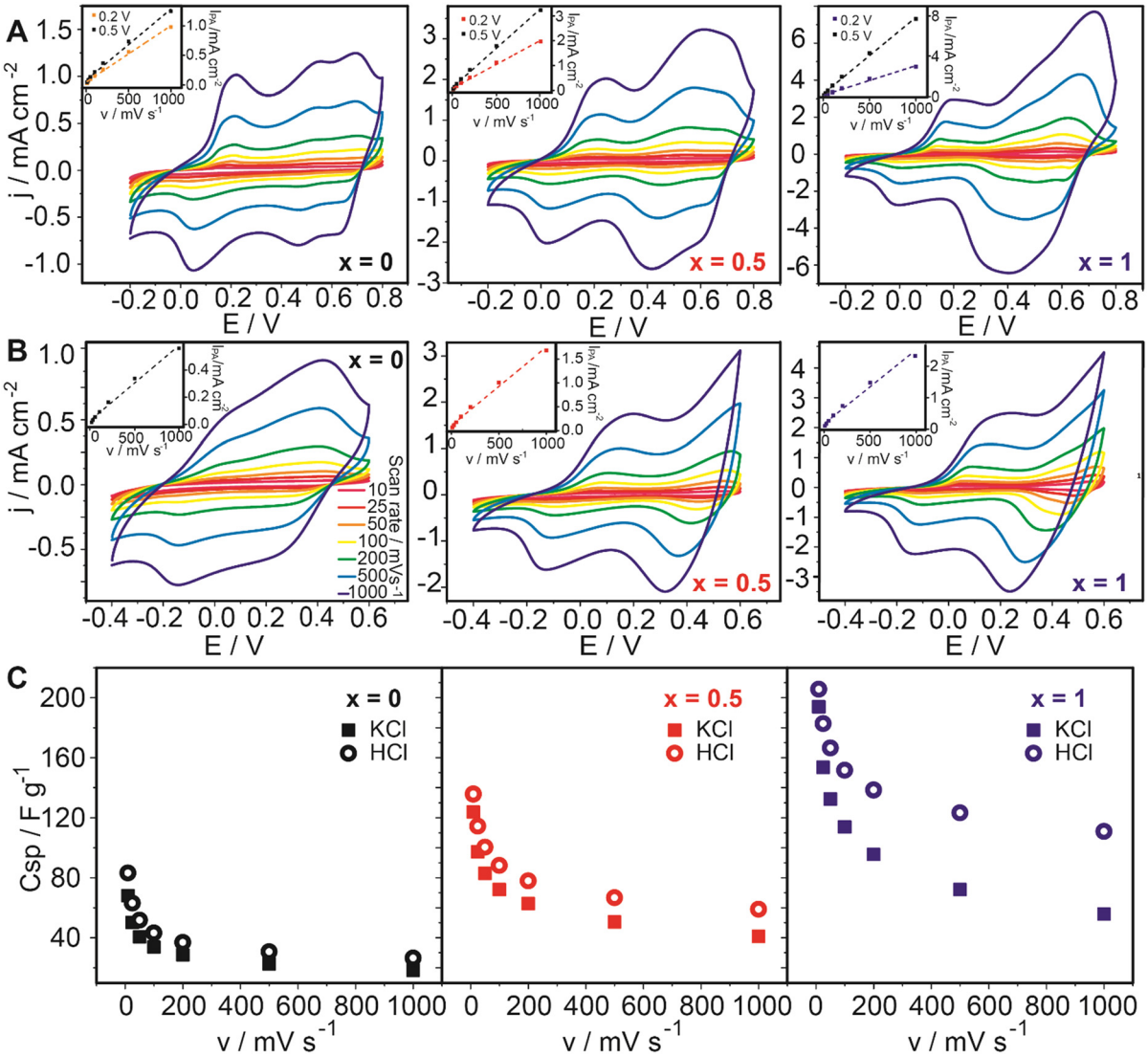

Fig. 3 (A) Cyclic voltammograms at different scan rates in 0.1 M HCl for x = 0 (left) x = 0.5 (center) and x = 1 (right). (B) Cyclic voltammograms at different scan rates in 0.1 M KCl for x = 0 (left) x = 0.5 (center) and x = 1 (right). Inset: peak current variation with scan rate increment. (C) Specific capacitance at each scan rate for x = 0 (left) x = 0.5 (center) and x = 1 (right) in both media.

and 193.9 F g^{-1} at 10 mV s^{-1} in acidic and neutral solution, respectively. For x = 0.5, $C_{CV,SP}$ values were 135.7 F g^{-1} and 123.9 F g^{-1} in HCl and KCl 0.1 M and the assemblies with x = 0 showed 83.1 F g^{-1} and 63.1 F g^{-1} in HCl and KCl, respectively. As previously observed, the voltammetric current and the specific capacitance of the composite-coated electrodes increase with the proportion of ferrocene-labelled surfactants.

Subsequently, and to study the ionic exchange in the assemblies during potential sweeping, simultaneous CV and film mass measurements were performed by electrochemical QCM (EQCM). Fig. 4A–C show the curves for the mass change as a function of the applied potential in 0.1 M KCl at 10 mV s^{-1} for the three systems with the corresponding voltammograms.

During the switching of electroactive films, mass changes occur due to ionic movement and exchange between the film and the solution for keeping the charge balance within the coating. Thus, the oxidation of the composite components (injection of positive charges from the electrode to the film) can be accompanied by the influx of anions or the efflux of cations to maintain charge balance. Conversely, the reduction (injection of electrons from the electrode to the film) can be accompanied by an influx of cations or an efflux of anions. Additionally, movement of solvent molecules takes place, both because ions are solvated and because oxidized and reduced states generally result in different levels of swelling. Next, as seen in Fig. 4A–C, the oxidation process in all three film assembly conditions is accompanied by a decrease in the mass of the assembly. This mass change can be interpreted by the flux of cations (and solvent) from the coating to the solution as a consequence of the oxidation of the conducting polymer and redox units. Conversely, during the reduction scan, the increment of the coating mass can be assigned to the flux of cations (and solvent) from the solution to the film.

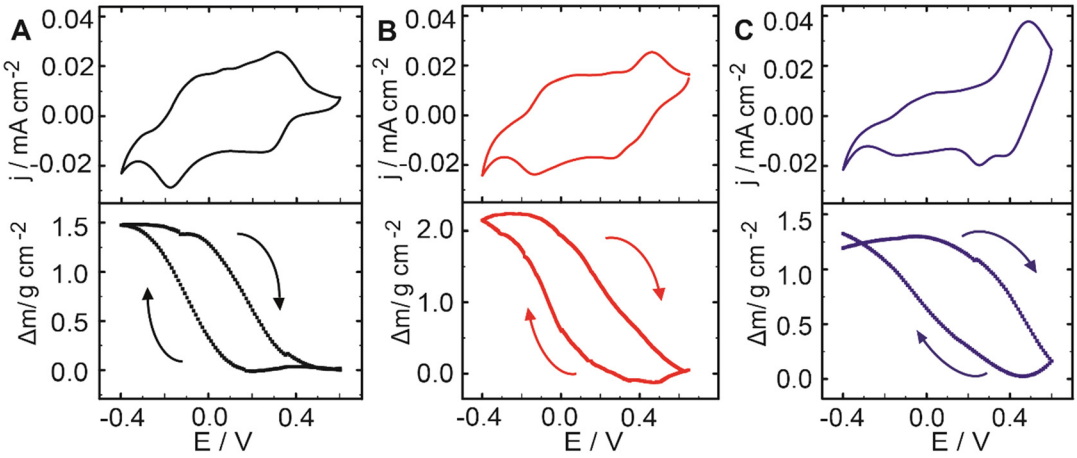

Fig. 4 Cyclic voltammetry and QCM mass change curves for the composite-modified electrodes at 10 mV s^{-1} in 0.1 M KCl (A) x = 0, (B) x = 0.5 and, (C) x = 1.

In the case of simple PANI films in acidic solutions, the oxidation process produces firstly proton expulsion and anion insertion as the electrode potential increases.[53] At intermediate pH values (between −1 and 2), there is an increased contribution of anion insertion to the charge-compensation process. In non-aqueous media, it seems that cations are retained inside the film and the charge is compensated for only by anion exchange. On the other hand, PANI-polyanion films are known to experience mixed proton–anion exchange in acidic media.[54] In the case of PANI-poly(vinylsulfonate) films, the dominant process of charge compensation at low pH is proton exchange, whereas, at intermediate pH values, anion insertion becomes important as well.

However, the PANI-PSS complex building block has an excess of negative charge even in acidic conditions. In this regard, the ζ-potential value of the PANI-PSS dispersion at pH 7 was determined to be −21.6 mV, while it was −13.8 mV in 0.5 M HCl (see the ESI†). Therefore, it can be deduced that charge compensation in this complex takes place by cation transport as mobile ions.[55–57] When reduction occurs, K^+ goes into the film to neutralize the excess negative charge of the PANI-PSS polymer complex. On the contrary, during the oxidation cations move from the film to the solution (Fig. 5A). Such a charge compensation mechanism has been previously observed in inorganic films of the negative complex hexacyanoferrate.[58]

An identical measure was carried out in 0.1 M HCl to confirm the cation movement (Fig. 5B). An example is shown in Fig. S7.† Even when considering hydration, previous research reported that H^+ hydrated molar mass is smaller than K^+.[58–60] As the same anion and concentration were employed, the differences in mass exchange in acidic (HCl) and neutral (KCl) solutions observed support the idea that charge balance is achieved by cation movement between the film and the solution.

The integrated charge was calculated from voltammograms, and the mass and charge variations were related to calculate the molar mass of the exchanged species. The obtained results are presented in Table S1,† showing an obtained average molar mass of 136 and 21.5 g mol^{-1} in 0.1 M KCl and 0.1 M HCl, respectively. This result indicates the effective exchange of hydrated K^+ and H^+ in neutral and acidic solutions, respectively.

Interestingly, it can be observed that the mass reduction during oxidation takes place even when the redox process is dominated by ferrocene redox chemistry, as in the case of the assembly with x = 1 for E applied >0.4 V (Fig. 4C). In this case, a sharper mass decrease is observed as a consequence of ferrocene oxidation. This is opposite to what has been observed in other LbL assemblies containing FcCTAB with

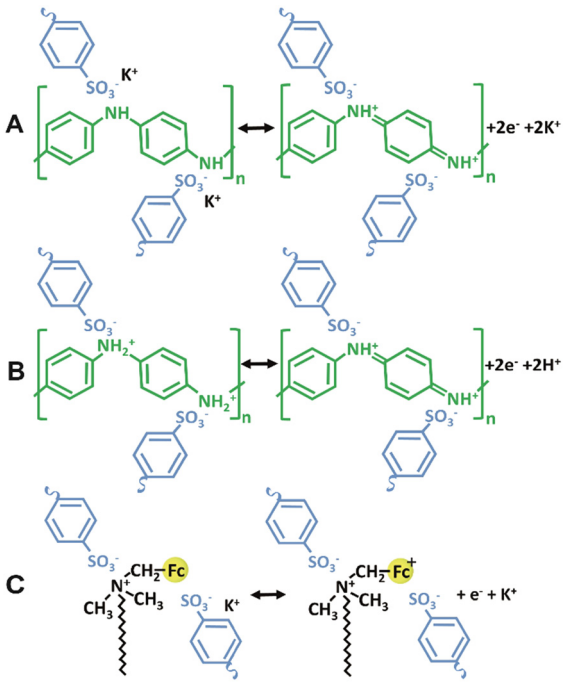

Fig. 5 Illustration of the ionic exchange in the electrochemical cycling for (A) PANI-PSS in KCl, (B) PANI-PSS in HCl and, and (C) FcCTAB in KCl.

scarcely charged polyacrylic acid, where charge compensation has been ascribed to anion movements.[46] This result suggests the intrinsic charge compensation of ferricenium moieties by the excess of PSS units (Fig. 5C).

Galvanostatic charge–discharge curves. To further study the energy storage performance of the assembled systems, galvanostatic charge–discharge cycles were performed at different current densities from 1.5 to 10 A g^{-1}. The current density was calculated employing the dry mass obtained in the QCM experiment. To calculate the specific capacitance ($C_{CG,SP}$/F g^{-1}) from charge–discharge curves, the following equation was employed (eqn (2)):

$$C_{CG,SP} = \frac{I\Delta t}{mV} \quad (2)$$

where ΔV is the potential window (V), m is the dry mass of the film measured by QCM (g), I is the current applied in the process (A), and Δt is the discharge time (s). Charge–discharge curves for an assembly of 11.5 bilayers and x = 1 in 0.1 M HCl and 0.1 M KCl are shown in Fig. 6A and B, respectively.

The variation of $C_{CG,SP}$ as a function of the current density in both media is reported in Fig. 6C. As could be expected, a decrease of $C_{CG,SP}$ values with increasing current density was noted. When measuring the curves in 0.1 M KCl, the obtained $C_{CG,SP}$ values ranged from 423.75 F g^{-1} to 125.0 F g^{-1} at 1.5 to 10 A g^{-1}, respectively.

Comparatively, the capacitive performance in charge–discharge cycles was outstanding in neutral medium. Considering the components of the assembly, the capacitive contributions of both nanocarbons (EDL-type) and ferrocene (redox-type) do not considerably change with pH. This leads to the possibility of employing the assembled electrodes in environmentally friendly neutral medium devices.

Subsequently, a comparative analysis was performed for the three systems with the aim of evaluating the ferrocene contribution to the capacitive response. As observed in the case of the voltammetric measurements, the capacitance obtained by GCD curves increases with the proportion of ferrocene-labelled surfactant both in neutral and acidic solutions (Fig. S8†). In this regard, the incorporation of ferrocene (Fc) in the supercapacitor assemblies has been observed to significantly improve their capacitive performance. This improvement can be attributed to several factors. Due to its inherent redox activity, the integration of ferrocene provides an additional pseudocapacitive contribution to the overall capacitance of the supercapacitor. In this regard, the reversible electron transfer between the ferrocene redox couple (Fe^{2+}/Fe^{3+}) enables faradaic charge storage, enhancing the overall energy storage capability of the system. On the other hand, the rapid electron transfer between ferrocene centers could promote efficient charge transfer kinetics at the electrode–electrolyte interface and within the coating. The presence of ferrocene could facilitate rapid electron transport, reducing the charge transfer resistance and enabling faster and more efficient charge storage and release processes.

Then, the present results indicate that the integration of ferrocene into the assemblies may constitute an efficient way to enhance the electrochemical capacitance performance of the composite materials for the development of aqueous electrolyte supercapacitors based on the integration of electroactive polymers and carbon nanomaterials.

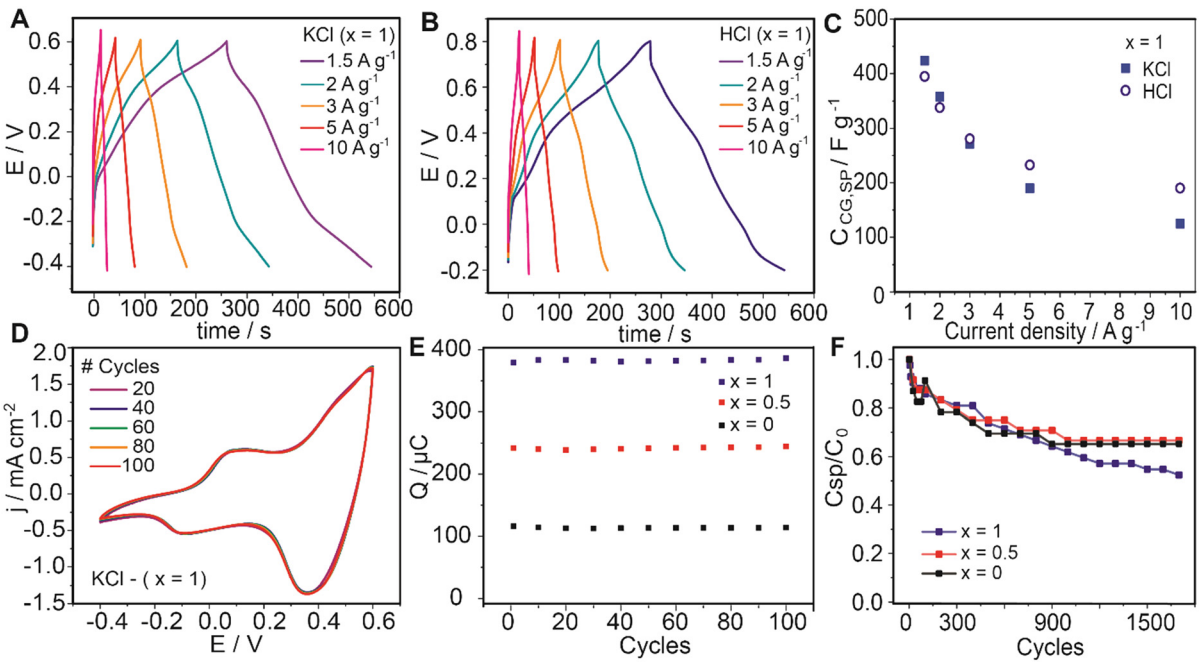

Fig. 6 Charge and discharge cycles for the 11.5 bilayer assembly with x = 1 in (A) HCl (0.1 M) and (B) KCl (0.1 M). (C) Specific capacitance values for different current densities. (D) Cyclic voltammograms for 100 cycles for x = 1 in 0.1 M KCl at 200 mV s^{-1}. (E) Integrated charge calculated for 100 curves from cyclic voltammetry. (F) Specific capacitance relative to the initial value for charge and discharge cycles up to 1700 cycles.

Table 1 Supercapacitor performance comparison considering works with the LbL assembly method

Layer by Layer combining	Electrolyte	Csp (F g^{-1})	Cycling stability	Ref.
Iron-decorated few-layer graphene/PANI : PSS (Au electrode)	0.1 M KCl 0.1 M HCl	659.2–1 A g^{-1} 768.6–1 A g^{-1}	86% 1600 cycles – 3 A g^{-1} 84% 1600 cycles – 3 A g^{-1}	35
Maghemite-magnetite (MAG)/reduced graphene oxide (rGO) (ITO glass)	0.5 M Na_2SO_3	691.29–5.6 A g^{-1}	87.5% 10 000 cycles – 56.4 A g^{-1}	63
PANI nanofiber spray/graphene oxide sheets spray (ITO glass)	0.5 M $LiClO_4$ in propylene carbonate	152–0.03 A g^{-1}	90% 1000 cycles – 2 A g^{-1}	64
Graphene nanosheets (GNS)/SnO_2 nanoparticles (ITO glass)	0.1 M H_2SO_4	471–1.28 A g^{-1}	72% 1000 cycles – 2.56 Ag^{-1}	65
Polyaniline nano fibers (PNFs)/MXene (ITO glass)	1 M $LiClO_4$ in propylene carbonate	208.37–0.1 A g^{-1}	56% 100 cycles – 10 A g^{-1}	66
Nanocarbon dispersed with FcCTAB/PANI-PSS (Au electrode)	0.1 M KCl aqueous	423.75 F g^{-1} – 1.5 A g^{-1}	52–67% 1700 cycles – 3 A g^{-1}	This work

Film stability and cyclability. Although ferrocene has been one of the most used moieties for redox labelling and mediation,[61] redox systems based on ferrocene typically exhibit low stability in aqueous media due to the susceptibility of the ferricenium species to react with O_2 in the presence of water, which leads to the loss of electroactive units.[62] For this reason, it is interesting to evaluate the stability and cyclability of the assemblies with ferrocene towards electrochemical switching. Therefore, the electrochemical stability was first tested by cyclic voltammetry. The voltammograms corresponding to 100 successive voltammetric cycles for the assembly with $x = 1$ are shown in Fig. 6D (results for $x = 0$ and $x = 0.5$ are presented in Fig. S9†), while the stability towards voltammetric cycling is presented in Fig. 6E in terms of the integrated voltammetric charge as a function of the number of cycles for the three different assemblies. Next, it can be observed that, independent of the amount of ferrocene present in the electrode coating, the electrochemical response remains unchanged even after 100 cycles between −0.4 and 0.6 V.

Afterward, we subjected the material to a more demanding test by studying the cyclability in terms of the capacitance retention determined from successive galvanostatic charge and discharge curves. The composite-modified electrodes were subjected to 1700 charge–discharge cycles from −0.1 to 0.6 V at 3 A g^{-1} in 0.1 M KCl. The evolution of the specific capacitance values relative to the initial capacitance for each assembly system is presented in Fig. 6F. From these experiments, 65%, 67%, and 52% retention of the initial specific capacitance were observed for the assemblies fabricated with $x = 0$, 0.5, and 1, respectively. Interestingly, these values suggest that increasing the ferrocene amount in the assembly does not change significantly the stability of the films under the electrochemical switching. Particularly in the case of the composite with $x = 0.5$, the good electrochemical stability indicates that the nanoarchitectonics of the assemblies prevent ferrocene degradation, taking into account the intrinsic instability of ferricenium in non-degassed neutral aqueous solutions. In this regard, electrochemically inactive blocks of carbon materials have been found to provide mechanical stability to assemblies with electroactive materials, increasing the resistance towards the expansion/shrinking caused by ions and solvent ingress/egress. On the other hand, the interactions with the counterparts (negatively charged PANI/PSS building block) could enhance the stability of the ferrocene moieties when oxidized to positive ferricenium (Fig. 5C).

Therefore, the electrochemical characterization of a coating incorporating ferrocene moieties demonstrates that the films retain suitable electrochemical stability, ensuring prolonged cycling stability and durability of the supercapacitor electrodes. It is seen that the reversible redox reactions of ferrocene can occur without significant degradation or loss of performance over multiple charge–discharge cycles, contributing to enhanced cycling stability and long-term reliability of the system.

Finally, the capacitive performance of the assemblies is compared with similar reported systems in Table 1, where reported LbL assemblies including carbon nanomaterials were selected from the bibliography. Our results indicate that the integration of carbon nanomaterials with ferrocene and PANI-PSS yields remarkable capacitive performance, particularly in neutral aqueous solution.

Conclusions

We have introduced a nanoarchitectonics approach for the integration of different building blocks by the LbL assembly method. This approach allows for the precise and efficient integration of various molecular-scale components, effectively capitalizing on the unique advantages of each material within the assembly. On the one hand, the nanoarchitectonic assembly leverages the conductivity, structural stability, and EDL capacitive contributions of carbon nanomaterials. Moreover, the conducting polymer block (PANI-PSS) exhibits a dual contribution, combining both EDLC and redox capacitance, enhancing the energy storage capacity. Finally, the ferrocene-labelled surfactant (FcCTAB) block introduces a third dimension of redox capacitance to the assembly.

In addition to the electrochemical investigations, EQCM has provided valuable information about the dynamic mass changes during the potential cycling of the supercapacitor electrodes, shedding light on the ionic exchange processes occurring within the assembly. The charge compensation mechanism,

specifically for the ferrocene-labelled surfactant (FcCTAB), displayed an intrinsic capacity for charge balance through cation transport as mobile ions. This behavior was distinct from that of simple PANI films in acidic solutions, where the charge compensation was dominated by proton expulsion and anion insertion. The results from the EQCM measurements corroborate the importance of cation movement between the film and the solution in achieving charge balance, particularly in the case of ferrocene-labelled surfactants.

Overall, the results demonstrated that the presence of ferrocene-labelled surfactant significantly contributed to the electrochemical connectivity within the assemblies. Cyclic voltammetry and galvanostatic charge–discharge measurements revealed that the specific capacitance of the composite-coated electrodes increased with the proportion of ferrocene-labelled surfactants, indicating the potential for improved charge accumulation. Moreover, the integration of ferrocene into the assemblies offered enhanced cycling stability, allowing for long-term reliability of supercapacitor electrodes.

This study demonstrates that the integration of the redox moiety significantly enhances the capacitive performance of the hybrid material in neutral solutions without noticeably affecting its structural stability and cyclability. Thus, the present approach synergistically combines the benefits of nanocarbon materials, electroactive polymers, and the faradaic contribution of the electroactive surfactant, leading to the creation of a supercapacitor material with excellent performance in neutral aqueous solution. The findings suggested that the rational incorporation of ferrocene moieties represents an efficient approach to enhance the electrochemical capacitance performance of composite materials for the development of aqueous electrolyte supercapacitors, which could find applications in secure energy storage for wearable devices.

Conflicts of interest

There are no conflicts to declare.

Acknowledgements

APM and GEF acknowledge scholarships from CONICET. OA, MR and WAM are staff members of CONICET and acknowledge the financial support from Universidad Nacional de La Plata (X867), CONICET (PIP-0370, PIP 11220210100209CO), and ANPCyT (PICT2018-00780, PICT2018-4684, PICT-2020-02468 and PICT-2021-GRFTI-00042).

Notes and references

1 B. E. Conway, *Electrochemical Supercapacitors*, Springer US, Boston, MA, 1999, vol. 25.
2 H. Chen, T. N. Cong, W. Yang, C. Tan, Y. Li and Y. Ding, *Prog. Nat. Sci.*, 2009, **19**, 291–312.
3 G. Z. Chen, *Int. Mater. Rev.*, 2017, **62**, 173–202.
4 A. González, E. Goikolea, J. A. Barrena and R. Mysyk, *Renewable Sustainable Energy Rev.*, 2016, **58**, 1189–1206.
5 L. D. Sappia, B. S. Pascual, O. Azzaroni and W. Marmisollé, *ACS Appl. Energy Mater.*, 2021, **4**, 9283–9293.
6 C. Lei, P. Wilson and C. Lekakou, *J. Power Sources*, 2011, **196**, 7823–7827.
7 P. Simon and Y. Gogotsi, *Nat. Mater.*, 2008, **7**, 845–854.
8 Z. Chang, Y. Yang, M. Li, X. Wang and Y. Wu, *J. Mater. Chem. A*, 2014, **2**, 10739–10755.
9 P. Chandrasekhar, *Conducting Polymers, Fundamentals and Applications*, Springer International Publishing, Cham, 2018.
10 M. Gerard, *Biosens. Bioelectron.*, 2002, **17**, 345–359.
11 W. A. Marmisollé and O. Azzaroni, *Nanoscale*, 2016, **8**, 9890–9918.
12 A. M. Bonastre, M. Sosna and P. N. Bartlett, *Phys. Chem. Chem. Phys.*, 2011, **13**, 5365.
13 G. Challa and Y. Y. Tan, *Pure Appl. Chem.*, 1981, **53**, 627–641.
14 A. P. Mártire, G. M. Segovia, O. Azzaroni, M. Rafti and W. Marmisollé, *Mol. Syst. Des. Eng.*, 2019, **4**, 893–900.
15 N. Parveen, S. A. Ansari, B. T. Al-Abawi and M. O. Ansari, *J. Energy Storage*, 2022, **55**, 105619.
16 N. Parveen, G. M. Alsulaim, S. A. Alsharif, H. H. Almutairi, H. A. Alali, S. A. Ansari and M. M. Ahmad, *J. Sci.: Adv. Mater. Devices*, 2023, **8**, 100591.
17 M. Z. Ansari, I. Hussain, D. Mohapatra, S. A. Ansari, R. Rahighi, D. K. Nandi, W. Song and S. Kim, *Adv. Sci.*, 2023, **2303055**, 1–44.
18 N. Parveen, M. O. Ansari, S. A. Ansari and P. Kumar, *Nanomaterials*, 2022, **13**, 105.
19 J. Scotto, G. E. Fenoy, D. Posadas, O. Azzaroni and W. A. Marmisolle, in *Conjugated Polymers for Next-Generation Applications*, Elsevier, 2022, pp. 175–218.
20 *Concepts and Design of Materials Nanoarchitectonics*, ed. O. Azzaroni and K. Ariga, The Royal Society of Chemistry, 2022.
21 E. Piccinini, M. Ceolín, F. Battaglini and O. Azzaroni, *ChemPlusChem*, 2020, **85**, 1616–1622.
22 O. Azzaroni and K. Ariga, *Mol. Syst. Des. Eng.*, 2019, **4**, 9–10.
23 M. Aono, Y. Bando and K. Ariga, *Adv. Mater.*, 2012, **24**, 150–151.
24 Z. Huang, L. Li, Y. Wang, C. Zhang and T. Liu, *Compos. Commun.*, 2018, **8**, 83–91.
25 X. Wang, D. Wu, X. Song, W. Du, X. Zhao and D. Zhang, *Molecules*, 2019, **24**, 2263.
26 Y. Yang, Y. Hao, J. Yuan, L. Niu and F. Xia, *Carbon*, 2014, **78**, 279–287.
27 S. Xiong, Y. Shi, J. Chu, M. Gong, B. Wu and X. Wang, *Electrochim. Acta*, 2014, **127**, 139–145.
28 Z. Wang, Q. Zhang, S. Long, Y. Luo, P. Yu, Z. Tan, J. Bai, B. Qu, Y. Yang, J. Shi, H. Zhou, Z.-Y. Xiao, W. Hong and H. Bai, *ACS Appl. Mater. Interfaces*, 2018, **10**, 10437–10444.
29 H.-P. Cong, X.-C. Ren, P. Wang and S.-H. Yu, *Energy Environ. Sci.*, 2013, **6**, 1185.
30 W. A. Marmisollé, E. Maza, S. Moya and O. Azzaroni, *Electrochim. Acta*, 2016, **210**, 435–444.
31 K. Ariga, J. P. Hill and Q. Ji, *Phys. Chem. Chem. Phys.*, 2007, **9**, 2319.
32 R. M. Iost and F. N. Crespilho, *Biosens. Bioelectron.*, 2012, **31**, 1–10.

33 G. Decher, B. Lehr, K. Lowack, Y. Lvov and J. Schmitt, *Biosens. Bioelectron.*, 1994, **9**, 677–684.
34 A. K. Sarker and J.-D. Hong, *Langmuir*, 2012, **28**, 12637–12646.
35 G. E. Fenoy, B. Van der Schueren, J. Scotto, F. Boulmedais, M. R. Ceolín, S. Bégin-Colin, D. Bégin, W. A. Marmisollé and O. Azzaroni, *Electrochim. Acta*, 2018, **283**, 1178–1187.
36 X. Wang, K. Gao, Z. Shao, X. Peng, X. Wu and F. Wang, *J. Power Sources*, 2014, **249**, 148–155.
37 M. Lorena Cortez, N. De Matteis, M. Ceolín, W. Knoll, F. Battaglini and O. Azzaroni, *Phys. Chem. Chem. Phys.*, 2014, **16**, 20844–20855.
38 M. L. Cortez, A. Lorenzo, W. A. Marmisollé, C. von Bilderling, E. Maza, L. Pietrasanta, F. Battaglini, M. Ceolín and O. Azzaroni, *Soft Matter*, 2018, **14**, 1939–1952.
39 A. Lorenzo, W. A. Marmisollé, E. M. Maza, M. Ceolín and O. Azzaroni, *Phys. Chem. Chem. Phys.*, 2018, **20**, 7570–7578.
40 E. Piccinini, J. S. Tuninetti, J. Irigoyen Otamendi, S. E. Moya, M. Ceolín, F. Battaglini and O. Azzaroni, *Phys. Chem. Chem. Phys.*, 2018, **20**, 9298–9308.
41 C. A. Goss, C. J. Miller and M. Majda, *J. Phys. Chem.*, 1988, **92**, 1937–1942.
42 J. S. Facci, P. A. Falcigno and J. M. Gold, *Langmuir*, 1986, **2**, 732–738.
43 G. E. Fenoy, B. Van der Schueren, J. Scotto, F. Boulmedais, M. R. Ceolín, S. Bégin-Colin, D. Bégin, W. A. Marmisollé and O. Azzaroni, *Electrochim. Acta*, 2018, **283**, 1178–1187.
44 D. Jariwala, V. K. Sangwan, L. J. Lauhon, T. J. Marks and M. C. Hersam, *Chem. Soc. Rev.*, 2013, **42**, 2824–2860.
45 T. Lee, S. H. Min, M. Gu, Y. K. Jung, W. Lee, J. U. Lee, D. G. Seong and B.-S. Kim, *Chem. Mater.*, 2015, **27**, 3785–3796.
46 E. Piccinini, G. A. González, O. Azzaroni and F. Battaglini, *J. Colloid Interface Sci.*, 2021, **581**, 595–607.
47 W.-S. Huang, B. D. Humphrey and A. G. MacDiarmid, *J. Chem. Soc., Faraday Trans. 1*, 1986, **82**, 2385.
48 S.-B. Yoon, E.-H. Yoon and K.-B. Kim, *J. Power Sources*, 2011, **196**, 10791–10797.
49 L. D. Arsov, W. Plieth and G. Koßmehl, *J. Solid State Electrochem.*, 1998, **2**, 355–361.
50 R. Mažeikien and A. Malinauskas, *Eur. Polym. J.*, 2002, **38**, 1947–1952.
51 J. Luo, S. Jiang, R. Liu, Y. Zhang and X. Liu, *Electrochim. Acta*, 2013, **96**, 103–109.
52 A. J. Bard, L. R. Faulkner and H. S. White, *Electrochemical methods: fundamentals and applications*, Wiley, 3rd edn, 2022.
53 C. Barbero, M. C. Miras, R. Kötz and O. Haas, *J. Electroanal. Chem.*, 1997, **437**, 191–198.
54 C. Barbero, M. C. Miras, O. Haas and R. Kötz, *J. Electrochem. Soc.*, 1997, **144**, 4170–4174.
55 L. P. Bauermann and P. N. Bartlett, *Electrochim. Acta*, 2005, **50**, 1537–1546.
56 X. Du, D. Zhang, X. Ma, W. Qiao, Z. Wang, X. Hao and G. Guan, *Electrochim. Acta*, 2018, **282**, 384–394.
57 B. Zhang, X. Du, X. Hao, F. Gao, D. Zhang, C. Liu and G. Guan, *J. Solid State Electrochem.*, 2018, **22**, 2473–2483.
58 M. A. Malik, K. Miecznikowski and P. J. Kulesza, *Electrochim. Acta*, 2000, **45**, 3777–3784.
59 H. Shao, K. Xu, Y.-C. Wu, A. Iadecola, L. Liu, H. Ma, L. Qu, E. Raymundo-Piñero, J. Zhu, Z. Lin, P.-L. Taberna and P. Simon, *ACS Energy Lett.*, 2020, **5**, 2873–2880.
60 K. Zheng, Y. Xian and Z. Lin, *Adv. Mater. Interfaces*, 2022, **9**, 1–7.
61 S. Takahashi and J. Anzai, *Materials*, 2013, **6**, 5742–5762.
62 A. Singh, D. R. Chowdhury and A. Paul, *Analyst*, 2014, **139**, 5747–5754.
63 M. A. Gross, K. A. Monroe, S. Hawkins, R. L. Quirino, S. G. C. Moreira, M. A. Pereira-da-Silva, S. V. de Almeida, R. C. Faria and L. G. Paterno, *J. Electroanal. Chem.*, 2022, **908**, 116123.
64 S. R. Kwon, J.-W. Jeon and J. L. Lutkenhaus, *RSC Adv.*, 2015, **5**, 14994–15001.
65 S. Patil, V. Patil, S. Sathaye and K. Patil, *RSC Adv.*, 2014, **4**, 4094–4104.
66 J. Yun, I. Echols, P. Flouda, S. Wang, A. Easley, X. Zhao, Z. Tan, E. Prehn, G. Zi, M. Radovic, M. J. Green and J. L. Lutkenhaus, *ACS Appl. Mater. Interfaces*, 2019, **11**, 47929–47938.